The Astrophysical Journal Letters, 921:L21 (6pp), 2021 November 1 https://doi.org/10.3847/2041-8213/ac2d30

The First Supermassive Black Hole Mass Measurement in Active Galactic Nuclei Using the Polarization of Broad Emission Line Mg II

Đorđe V. Savić[1,2], Luka Č. Popović[2,3], and Elena Shablovinskaya[4]
[1] Institut d'Astrophysique et de Géophysique, Université de Liège Allée du 6 Août 19c, 4000 Liège, Belgium; djsavic@aob.rs
[2] Astronomska opservatorija, Beograd Volgina 7, 11060 Belgrade, Serbia
[3] Department of Astronomy, Faculty of Mathematics, University of Belgrade Studentski trg 16, 11000 Belgrade, Serbia
[4] Astrophysical Observatory of the Russian Academy of Sciences Nizhnij Arkhyz, Karachaevo-Cherkesia 369167, Russia
Received 2021 June 4; revised 2021 September 22; accepted 2021 September 23; published 2021 November 2

Abstract

Spectropolarimetric efforts in the last few years have developed an efficient method that is based on the profiles of the polarization plane position angle of broad emission lines in active galactic nuclei. Here we present black hole measurements of SBS 1419+538 using spectropolarimetric observations in the Mg II spectral band. The observations are performed by the 6 m telescope of the Special Astrophysical Observatory of the Russian Academy of Sciences (SAO RAS) using SCORPIO-2. We found good agreement for this object's estimated supermassive black hole mass using spectropolarimetry compared with the mass obtained using other methods.

Unified Astronomy Thesaurus concepts: Spectropolarimetry (1973); Supermassive black holes (1663); Active galaxies (17); Seyfert galaxies (1447); Quasars (1319); Polarimetry (1278)

1. Introduction

According to the standard paradigm, active galactic nuclei (AGNs) are powered by the accretion of gas onto the supermassive black hole (SMBH), which resides at the galaxy's center (Salpeter 1964; Zel'dovich & Novikov 1964; Lynden-Bell 1969). Due to the finite, but low viscosity, of the gas, the gas temperature increases and the angular momentum is transferred outwards, providing a slow, but steady inflow (Shakura & Sunyaev 1973). The gravitational binding energy is converted into an enormous amount of radiation, which ranks AGNs as the most luminous steady sources observed (Padovani 2017). SMBHs actively shape the environment in their vicinity, but also on kiloparsec scales, through a process known as AGN feedback (Fabian 2012), which plays an important role in the host galaxy evolution (Kormendy & Ho 2013; Heckman & Best 2014). Therefore, reliable SMBH mass estimation is an important problem in modern astrophysics.

Many methods with different approaches have been developed in the past few decades and have been extensively discussed in the literature (e.g., Peterson 2014; Popović 2020, and references therein). Broad emission lines in AGNs have been widely used for measuring SMBH mass, most often in long-term reverberation mapping campaigns (Blandford & McKee 1982; Peterson 1993; Kaspi et al. 2000; Bentz et al. 2013; Du et al. 2016, 2018; Shapovalova et al. 2019, etc.).

When the polarized emission is taken into account, the broad line spectropolarimetry allows us to measure the SMBH mass with single-epoch observations (Afanasiev & Popović 2015, hereafter AP15 method). This method assumes that equatorial scattering of the inner side of the dusty torus is the dominant polarization mechanism (Smith et al. 2005; Savić et al. 2018, 2020; Lira et al. 2020) and is in good agreement with other methods (Afanasiev et al. 2019). In order to use the AP15 method, it is required that the distance (R_{sc}) between the SMBH and the scattering region is known. In the case of the Keplerian-like motion in combination with the equatorial scattering of the BLR light, the relation between velocities and polarization angle ($\tan\varphi$) across the broad line is:

$$\log\left(\frac{V_i}{c}\right) = a - b \cdot \log\left(\tan(\Delta\varphi_i)\right), \quad (1)$$

where c is the speed of light, and constant a depends on the BH mass $\mathcal{M}_{bh}$ as

$$a = 0.5 \log\left(\frac{G\mathcal{M}_{bh}\cos^2(\theta)}{c^2 R_{sc}}\right), \quad (2)$$

where G is the gravitational constant and θ is the angle between the BLR disk, and the scattering region is assumed to be $\theta \sim 0$ in the case of equatorial scattering and therefore the BH mass estimate is independent from the inclination. The constant b is close to 0.5 for the dominant Keplerian-like motion. One of the advantages is that this method can be applied to Mg II, C III, and C IV broad lines, which would correspond to distant objects at high redshift, if these lines are observed in the optical spectral range. In this work, we report the first spectropolarimetric observations of the Mg II line for a distant AGN SBS 1419+538 and we compare the SMBH mass estimated using the AP15 method with the estimates provided by different authors using other methods (most notably reverberation mapping).

2. Polarimetric Observations of the Mg II Spectral Line

In order to test the model of polarization changes for the Mg II line, in 2019 February we carried out the spetropolarimetric observations of the quasar SBS 1419+538. SBS 1419+538 (R. A. $14^h\,21^m\,06\overset{s}{.}9$, decl. $+53°\,37'\,45\overset{''}{.}2$, J2000) is a bright quasar (16.8 mag in the g-sdss band) at the redshift $z = 1.862$ determined for the first time via the Second Byurakan Survey (Stepanian et al. 1993). The SDSS spectra of the quasar show broad (FWHM $\sim 5000\,\mathrm{km\,s^{-1}}$) components of the Mg II and CIII] in the optical range (Schneider et al. 2005; Shen et al. 2011).

SBS 1419+538 was observed with the 6 m telescope BTA of the Special Astrophysical Observatory of the Russian Academy of Sciences (SAO RAS) with the focal reducer SCORPIO-2 (Afanasiev & Moiseev 2011). We used a 1″ slit and a volume phase holographic grating covering the 5800–9500 Å range with a maximum at 7350 Å to obtain the spectrum images. The double Wollaston prism divided the image of the entrance pupil according to four polarization directions—0°, 90°, 45°, and 135°. Then the parameters of the linear polarization and intensity—the Stokes parameters Q, U, and I were obtained simultaneously and are equal to:

$$Q(\lambda) = \frac{I_0(\lambda) - I_{90}(\lambda)K_Q(\lambda)}{I_0(\lambda) + I_{90}(\lambda)K_Q(\lambda)}, \quad (3)$$

$$U(\lambda) = \frac{I_{45}(\lambda) - I_{135}(\lambda)K_U(\lambda)}{I_{45}(\lambda) + I_{135}(\lambda)K_U(\lambda)}, \quad (4)$$

$$I(\lambda) = I_0(\lambda) + I_{90}(\lambda)K_Q(\lambda) + I_{45}(\lambda) + I_{135}(\lambda)K_U(\lambda), \quad (5)$$

where K_Q and K_U are the coefficients of the channel transmission, and I_0, I_{90}, I_{45}, and I_{135} correspond to the different polarization directions. Using K_Q and K_U coefficients one can minimize the influence of variable atmospheric depolarization (see Afanasiev & Amirkhanyan 2012 for more details). Then the polarization degree P and polarization angle φ are obtained from the following relations:

$$P(\lambda) = \sqrt{Q^2(\lambda) + U^2(\lambda)}, \quad (6)$$

$$\varphi(\lambda) = \frac{1}{2}\arctan[U(\lambda)\Big/Q(\lambda)] + \varphi_0, \quad (7)$$

where φ_0 is the zero-point of the polarization angle. To correct the device's spectral sensitivity and to find φ_0, the nonpolarized spectrophotometric and polarized standards were observed before the object. The polarimetric accuracy was dependent on variations of the atmospheric depolarization. Due to the high galactic latitude of the quasar ($b \sim 60°$) the ISM polarization is neglected. The observations of the object were performed in a series of 16 frames with 300 s exposure times in order to make robust statistical estimations. The observational techniques and analysis method have been described in more detail in several papers (see, e.g., Afanasiev & Amirkhanyan 2012; Afanasiev et al. 2014; Afanasiev & Popović 2015; Afanasiev et al. 2019) and will not be repeated.

3. Results

The extracted spectra and observed polarization parameters are shown in Figure 1. The first panel shows the total flux in the spectral region near the broad Mg II line 7500 Å to 8500 Å with 2 Å spectral resolution. The continuum emission is approximated here with a linear regression plotted with a dashed line. The second and third panels show the Stokes parameters Q and U, respectively. The polarization degree P and the polarization angle φ are given in the fourth and fifth panels. The Stokes parameters Q and U, P and φ are binned over 10 Å and depend on the wavelength. For each bin, the value was calculated as a robust average in the two-dimensional array of size 10 Å by 16 exposures; the error bars are equal to the 1σ level as a robust standard deviation. A 2σ rejection threshold was used in order to avoid the influence of the outlier points (less than 1% mostly

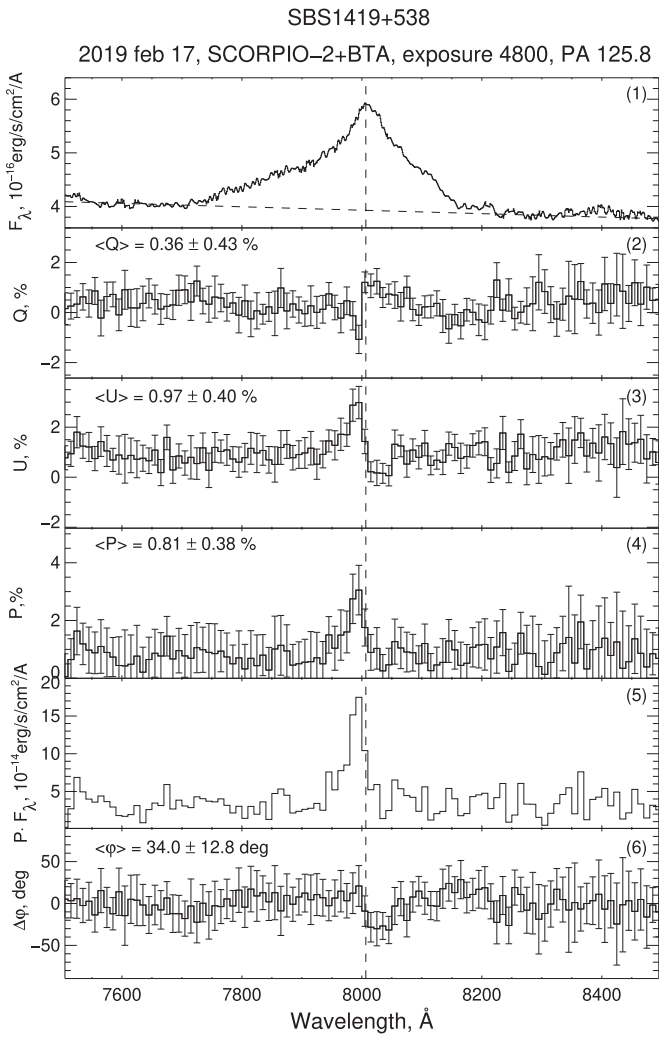

Figure 1. The Mg II spectral region (first panel), the Q and U Stokes parameters (second and third panels), and polarization degree and polarization angle (fourth and fifth panels) across the line profile.

due to the cosmic rays' hints). The average values of the parameters $\langle Q\rangle$, $\langle U\rangle$, $\langle P\rangle$, and $\langle\varphi\rangle$ are also given in the figure.

As the measured value of polarization is small and is comparable with the errors, the value of polarization degree P is biased. The correction of P to the bias was made according to the formula given in Simmons & Stewart (1985):

$$P = \sqrt{P_{\rm obs}^2 - 1.41\sigma_P^2}, \quad (8)$$

where $P_{\rm obs}$ is the measured value of polarization and σ_P is its error. Therefore, there are unbiased values of P given in Figure 1.

The polarization profile of Mg II being single peaked and blueshifted may indicate some complex structures in the Mg II BLR, such as, e.g., outflowing/inflowing BLR (Popović et al. 2019; Savić et al. 2020) or a more complex two-component model (Popović et al. 2004), which can hide the expected two peaks of the polarized profile in the case of disk-like motion (Savić et al. 2020). However, in the case of pure disk-like motion, the single-peaked polarized profile can be detected in the case of lower viewing inclinations (see Figure 2 of Savić et al. 2020). Moreover, a single-peaked polarized line profile does not exclude dominant disk-like motion, and most equatorial scattered type 1 AGNs in the sample of Afanasiev et al. (2019) have single-peaked polarized profiles, but the

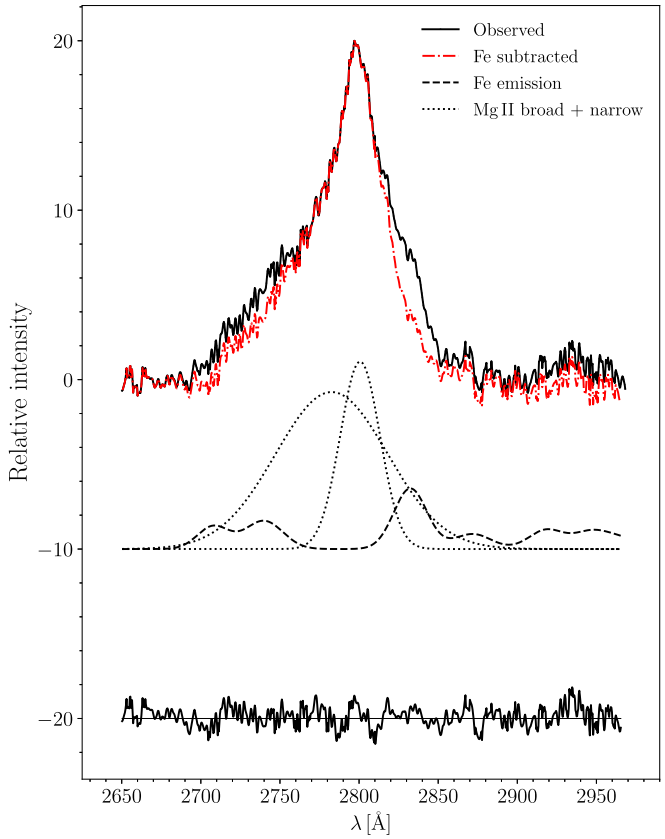

Figure 2. Decomposition of Mg II line emission. Top: solid black line denotes the observed spectrum; dashed red line is the Mg II profile after Fe II subtraction. Middle: broad and narrow Gaussian components of the Mg II line (dotted line) with the contribution of the total UV Fe II emission (dashed black line). Residuals are shown on the bottom.

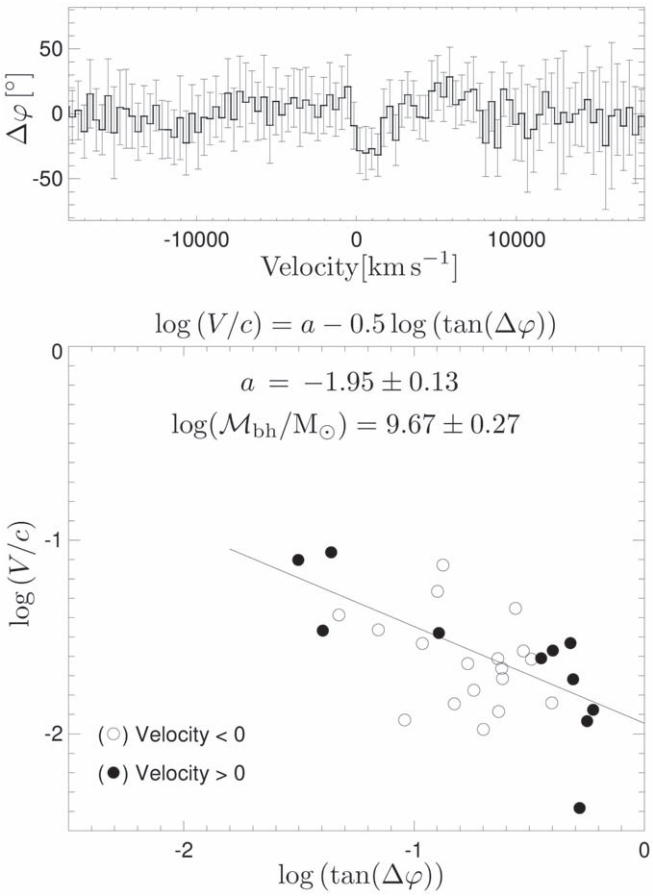

Figure 3. The relation $\log(V/c)$ vs. $\log(\tan[\Delta\varphi])$ after rest frame correction. The velocity range for fitting is the interval between -10^4 km s^{-1} and 10^4 km s^{-1}.

polarization angle swing indicates Keplerian-like motion in the BLR (see Figures 4–9 of Afanasiev et al. 2019).

It is well-known that there is strong iron emission underlying the Mg II line that also arises from the BLR. Estimating iron emission is a nontrivial task and much effort has been invested in solving this problem (Popović et al. 2019, and references therein). We used an improved model by Kovačević-Dojčinović & Popović (2015) that covers the spectral range between 2650–3050Å. Details regarding this model were extensively described by Popović et al. (2019). An illustration of the Mg II decomposition is shown in Figure 2. A blue asymmetry is dominant after Fe II subtraction, indicating outflow, which is also seen in the blueshifted polarized profile.

To obtain the SMBH mass according to the polarization properties of the equatorially scattered emission in the Mg II line by the method given in Afanasiev & Popović (2015) one should estimate the radius of the scattering region $R_{\rm sc}$. In Afanasiev et al. (2019) the dependency connecting $R_{\rm sc}$ in AGN and the luminosity at 1516 Å was revealed:

$$\log R_{\rm sc} = -(15.60 \pm 0.54\ ) + (0.40 \pm 0.01\ )\log(\lambda L_{1516\,\text{Å}}). \quad (9)$$

Because the spectropolarimetric observations given here have relatively bad photometric bounding due to the slit loses, more confident estimations of luminosity of SBS 1419+538 should be used. According to Shen et al. (2016) $\lambda L_{1350} = 8.9 \cdot 10^{46}$ erg s^{-1} and $\lambda L_{1700} = 7.2 \cdot 10^{46}$ erg s^{-1}. As the continuum spectra slope in the spectral range is not steep let us consider $\lambda L_{1516} \approx 8 \cdot 10^{46}$ erg s^{-1}, and according to the dependency 9, $R_{\rm sc}$ is equal to:

$$R_{\rm sc} = 2041 \pm 683 \ \text{lightdays}. \quad (10)$$

The error of $R_{\rm sc}$ was estimated by the bootstrapping method (Efron 1979) and includes the errors of the coefficients from Equation (9). The asynchronism of the continuum luminosity taken from Shen et al. (2016) with respect to the spectropolarimetric observation from the given work and the $\lambda L_{1516\,\text{Å}}$ uncertainty being smaller than the coefficient error were not taken into account.

We applied the AP15 method to find the black hole mass, and, as can be seen from Figure 3, for the Mg II line in the spectrum of SBS 1419+538 the observational data could be fitted with a linear function with the regression coefficient $a = -1.95 \pm 0.13$. Note here that the computed slope of the b coefficient is 0.46 ± 0.11, so practically it was assumed to be identically equal to 0.5, which corresponds to the case of Keplerian motion. Assuming that the BLR is coplanar with the dust scattering region ($\cos^2(\theta) = 1$, see AP15 for more details), we determined that the SMBH mass is:

$$\log(\mathcal{M}_{\rm bh}/M_\odot) = 9.67 \pm 0.27. \quad (11)$$

To examine the result we also tried other methods of indirect mass measurements. The mass could be estimated from the virial theorem. To calculate the virial product one should

Table 1
Previous Measurements of SBS 1419+538 Found in the Literature

Reference	z	$\log \lambda L_{1350}$ erg s^{-1}	$\log \lambda L_{1700}$ erg s^{-1}	$\log \lambda L_{3000}$ erg s^{-1}	$\log L_{\mathrm{Mg\,II}}$ erg s^{-1}	FWHM Mg II km s^{-1}	FWHM C IV km s^{-1}	R_{BLR} ld	$\log(\mathcal{M}_{\mathrm{bh}})$ $M_{\odot}$
Shen et al. (2008)	1.8583			46.89		8557			10.168
Shen et al. (2011)	1.8577	47.035 ± 0.004		46.902 ± 0.011	44.97 ± 0.01	5889.7 ± 821.6	3352.5 ± 106.5		10.08 ± 0.15
Rafiee & Hall (2011)	1.8583			46.88				813	9.91
Shen et al. (2016)	1.863	46.9482 ± 0.0022	46.8588 ± 0.0012	46.7887 ± 0.0004					
Grier et al. (2019)	1.862	46.948 ± 0.003							9.31
This work	1.862				45.50 ± 0.02	4791 ± 552		1195^{+936}_{-541}	9.67 ± 0.27

Note. Columns from left to right: references, redshift, continuum luminosities at 1350, 1700, and 3000, bolometric luminosity, full width at half maximum (FWHM) of the Mg II and C IV, the broad line region radius, and estimated SMBH mass. We ignore the error bars that were not given by previous authors. All SMBH measurement were obtained by a single-epoch approach.

estimate the velocity dispersion of the broad emission line. We measured the FWHM $= 4791 \pm 552$ km s^{-1} and line dispersion $\sigma = 2275 \pm 263$ km s^{-1} after subtracting the Fe II contribution to the Mg II line using the UV Fe II model given in Popović et al. (2019).[5]

The size of the BLR region in the Mg II line is estimated using the empirical BLR radius—luminosity (R-L) relation (see Czerny et al. 2019; Popović 2020). We used an updated R-L relation at 3000 Å given by Zajaček et al. (2020). The estimation of the quasar luminosity was obtained from Shen et al. (2016), $\lambda L_{3000} = 6.1\text{d}46$ erg s^{-1}. The BLR size was estimated as $R_{\rm BLR} = 1195^{+936}_{-541}$ light days. Therefore, the relation between the scattering region size and the BLR size is $R_{\rm sc}/R_{\rm BLR} \approx 1.7 \pm 0.7$. This value is in good agreement with the mean ratio obtained by Afanasiev et al. (2019) as well as models by Savić et al. (2018) for which the ratio is expected to be in the range between 1.5 and 2.5.

The virial product could be calculated:

$$VP = \frac{\sigma^2 R_{\rm BLR}}{G} \approx 1.2 \times 10^9 M_{\odot}. \quad (12)$$

From the profile of the polarization angle, it is possible to determine the BLR direction of rotation. A maximum of the polarization angle in the blue wing of the line followed by the minimum in the red wing corresponds to the counterclockwise rotation of the central engine (Savić et al. 2018).

4. Discussion and Conclusions

Magnesium lines are often associated with powerful outflows in addition to Keplerian motion (Laha et al. 2021). The outflows may be triggered by radiation pressure from the accretion disk and recently have been directly observed (Miyauchi & Kishimoto 2020). In our previous works (Savić et al. 2018, 2020), we found that the AP15 method may be used with sufficient accuracy even if the outflows are present. The main uncertainty in the SMBH mass estimate is proportional to the radius of the scattering region for which we lack direct measurements. Instead, we rely on various scaling relations that typically involve measured UV, optical, or infrared luminosity at certain wave bands (Koshida et al. 2014; Afanasiev et al. 2019), which in principle increase the error of the estimated SMBH mass. Another difficulty that arises using the current observational technique is the upper magnitude limitation. Due to the high redshift of the observed object, we are prone to observe only the brightest quasars in the spectropolarimetry mode.

As follows from the description of the spectropolarimetric AP15 method, the two main advantages of the approach are the use of single-epoch observations and the independence from the orientation of the AGN relative to the observer. Due to the accumulated data on AGN reverberation mapping and the relatively high statistical accuracy of the luminosity dependences on the BLR size, the mass estimate can also be obtained from single observations. In Table 1 we report previous measurements of SBS 1419+538 found in literature. Earlier SMBH estimates using data from the SDSS campaign are close to $\log(\mathcal{M}_{\rm bh}/\ {\rm M}_{\odot}) \approx 10$ (Shen et al. 2008, 2011; Rafiee & Hall 2011; Grier et al. 2019). Generally, our results are in good agreement with the SMBH estimates. However, this estimate will depend on an unknown dimensionless factor $f \approx 1 \sim 10$, depending on the system orientation and geometry (Kaspi et al. 2000; Onken et al. 2004; Bentz et al. 2013). Thus, the mass estimation error can reach 1 order of magnitude. A joint approach combining several types of mass estimation allows us to give more accurate and independent estimates of the masses.

A comparison of two independent estimates of the masses of the SMBH in Equations (10) and (12) allows us to estimate the dimensionless factor f, which in this case is equal to approximately 4. This value of the factor is close to the average value ($f = 5.5$ is assumed for most AGNs, see Onken et al. 2004). Even if we assume that the $\mathcal{M}_{\rm bh}$ obtained by spectropolarimetry is overestimated by 35%, it is assumed that according to the results of numerical modeling (Savić et al. 2020) the factor f is expected to be equal to approximately 3. Note here that the 2 times difference between the mass estimate given in this article and in Grier et al. (2019) can also be explained by an incorrect choice of f.

An additional difficulty of the AP15 method is the need to estimate the inner radius of the dusty torus where equatorial scattering is probably starting (see Figure 1 in Shablovinskaya et al. 2020). There are no estimates of the radius of the dust torus in the IR range for the quasar SBS 1419+538 in the literature, and the results of the SDSS-RM campaign have not been published yet. Therefore, we used the empirical relation 9. Undoubtedly, this worsens the accuracy of the estimated size of $R_{\rm sc}$. However, the $R_{\rm sc}/R_{\rm BLR}$ ratio is close to the theoretical prediction, which indicates that the error in determining $R_{\rm sc}$ is not larger than 30%, i.e., lies within the accuracy of the AP15 method for the Mg II line (Savić et al. 2020). In the future, the data of the SDSS-RM project or the results of the application of a new method for estimating the scattering region by reverberation mapping in polarized light (Shablovinskaya et al. 2020) will help to improve the accuracy of the mass estimate.

We apply for the first time the AP15 method for the Mg II broad line. Future work using the existing facility will include additional spectropolarimic observations of distant quasars focusing on C III and C IV emission lines. Current limitations will be largely surpassed with a next-generation instrument POLLUX (Muslimov et al. 2018) that will be aboard the mission LUVOIR (Large UV/Optical/IR Surveyor, The LUVOIR Team 2019).

We dedicate this work to Viktor Leonidovich Afanasiev[†6] who performed observations and data reduction as well as the set up of the polarimetric observations at SAO that provided these measurements. This work was supported by the F.R.S. FNRS under grant PDR T.0116.21; the Ministry of Education and Science Republic of Serbia through the project №̲ 451-03-68/2020-14/200002. Đ.S. thanks the RFBR for the realization of the three month short-term scientific visit at SAO funded by the grant №̲ 19-32-50009. E.S. thanks the grant of Russian Science Foundation project number №̲ 20-12-00030 "Investigation of geometry and kinematics of ionized gas in active galactic nuclei by polarimetry methods," which supported the spectropolarimetric data analysis.

References

Afanasiev, V. L., & Popović, L. Č. 2015, ApJL, 800, L35
Afanasiev, V. L., & Amirkhanyan, V. R. 2012, AstBu, 67, 438
Afanasiev, V. L., & Moiseev, A. V. 2011, BaltA, 20, 363
Afanasiev, V. L., Popović, L. Č., & Shapovalova, A. I. 2019, MNRAS, 482, 4985

[5] Models of the UV Fe II can be found at http://servo.aob.rs/FeII_AGN/link7.html.

[6] Deceased on 2020 December 21.

Afanasiev, V. L., Popović, L. Č., Shapovalova, A. I., Borisov, N. V., & Ilić, D. 2014, MNRAS, 440, 519
Bentz, M. C., Denney, K. D., Grier, C. J., et al. 2013, ApJ, 767, 149
Blandford, R. D., & McKee, C. F. 1982, ApJ, 255, 419
Czerny, B., Olejak, A., Rałowski, M., et al. 2019, ApJ, 880, 46
Du, P., Lu, K.-X., Hu, C., et al. 2016, ApJ, 820, 27
Du, P., Zhang, Z.-X., Wang, K., et al. 2018, ApJ, 856, 6
Efron, B. 1979, AnSta, 7, 1
Fabian, A. C. 2012, ARA&A, 50, 455
Grier, C. J., Shen, Y., Horne, K., et al. 2019, ApJ, 887, 38
Heckman, T. M., & Best, P. N. 2014, ARA&A, 52, 589
Kaspi, S., Smith, P. S., Netzer, H., et al. 2000, ApJ, 533, 631
Kormendy, J., & Ho, L. C. 2013, ARA&A, 51, 511
Koshida, S., Minezaki, T., Yoshii, Y., et al. 2014, ApJ, 788, 159
Kovačević-Dojčinović, J., & Popović, L. Č. 2015, ApJS, 221, 35
Popović, L. Č., Kovačević-Dojčinović, J., & Marčeta-Mandić, S. 2019, MNRAS, 484, 3180
Laha, S., Reynolds, C. S., Reeves, J., et al. 2021, NatAs, 5, 13
Lira, P., Goosmann, R. W., Kishimoto, M., & Cartier, R. 2020, MNRAS, 491, 1
Lynden-Bell, D. 1969, Natur, 223, 690
Popović, L. Č., Mediavilla, E., Bon, E., & Ilić, D. 2004, A&A, 423, 909
Miyauchi, R., & Kishimoto, M. 2020, ApJ, 904, 149
Muslimov, E., Bouret, J.-C., Neiner, C., et al. 2018, Proc. SPIE, 10699, 1069906
Onken, C. A., Ferrarese, L., Merritt, D., et al. 2004, ApJ, 615, 645
Padovani, P. 2017, FrASS, 4, 35
Peterson, B. M. 1993, PASP, 105, 247
Peterson, B. M. 2014, SSRv, 183, 253
Popović, L. Č. 2020, OAst, 29, 1
Rafiee, A., & Hall, P. B. 2011, ApJS, 194, 42
Salpeter, E. E. 1964, ApJ, 140, 796
Savić, D., Goosmann, R., Popović, L. Č., Marin, F., & Afanasiev, V. L. 2018, A&A, 614, A120
Schneider, D. P., Hall, P. B., Richards, G. T., et al. 2005, AJ, 130, 367
Savić, Đ. J., Popović, L. Č., Shablovinskaya, E., & Afanasiev, V. L. 2020, MNRAS, 497, 3047
Shablovinskaya, E. S., Afanasiev, V. L., & Popović, L. č. 2020, ApJ, 892, 118
Shakura, N. I., & Sunyaev, R. A. 1973, A&A, 500, 33
Shapovalova, A. I., Popović, L. Č., et al. 2019, MNRAS, 485, 4790
Shen, Y., Greene, J. E., Strauss, M. A., Richards, G. T., & Schneider, D. P. 2008, ApJ, 680, 169
Shen, Y., Horne, K., Grier, C. J., et al. 2016, ApJ, 818, 30
Shen, Y., Richards, G. T., Strauss, M. A., et al. 2011, ApJS, 194, 45
Simmons, J. F. L., & Stewart, B. G. 1985, A&A, 142, 100
Smith, J. E., Robinson, A., Young, S., Axon, D. J., & Corbett, E. A. 2005, MNRAS, 359, 846
Stepanian, J. A., Lipovetsky, V. A., Chavushian, V. H., Erastova, L. K., & Balayan, S. K. 1993, BSAO, 36, 5
The LUVOIR Team 2019, arXiv:1912.06219
Zajaček, M., Czerny, B., Martinez-Aldama, M. L., et al. 2020, ApJ, 896, 146
Zel'dovich, Y. B., & Novikov, I. D. 1964, SPhD, 9, 246